JACS Au
AN OPEN ACCESS JOURNAL OF THE AMERICAN CHEMICAL SOCIETY

pubs.acs.org/jacsau
Letter

Formamide Electrosynthesis from Methanol and Ammonia in Water over Pr-Doped MnO_2

Jiewei Zhu, Jiang Shao, Bai-An Shen, Jixiang Chen, Yifu Yu, Shuyan Song, Xin-Bo Zhang, Bin Zhang,* and Bo-Hang Zhao*

Cite This: *JACS Au* 2023, 3, 2987−2992
Read Online
ACCESS | Metrics & More | Article Recommendations | Supporting Information

ABSTRACT: A rare earth element doping strategy is reported to boost the activity and enhance the stability of MnO_2 for selective formamide production through electrocatalytic oxidation coupling (EOC) of methanol and ammonia. MnO_2 doped with 1% Pr was selected as the best candidate with an optimized formamide yield of 211.32 μmol cm^{-2} h^{-1}, a Faradaic efficiency of 22.63%, and a stability of more than 50 h. The easier formation of Mn^{6+} species and the lower dissolution rate of Mn species over Pr-doped MnO_2 revealed by in situ Raman spectra were responsible for the boosted formamide production and enhanced stability. In addition, a two-electrode flow electrolyzer was developed to integrate EOC with C_2H_2 semihydrogenation for simultaneously producing value-added products in both the anode and cathode.

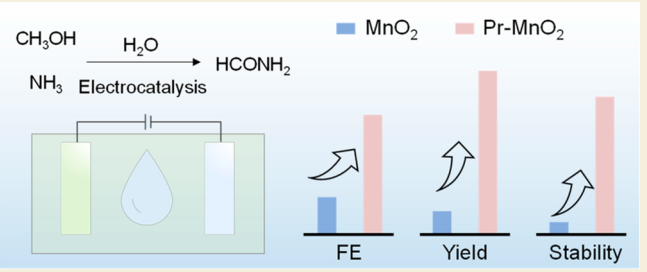

KEYWORDS: *electrosynthesis, formamide, water, rare earth, doping*

Amides, as a very important class of compounds in chemistry, medicine, and the agriculture industry, have been studied extensively over the past century.[1−4] Formamide, for example, is produced and consumed in millions of tons worldwide every year and is widely used in pesticides, dyes, pigments, flavors, organic synthesis, and pharmaceuticals.[5,6] Currently, formamide is mostly synthesized from CO and ammonia (NH_3), which not only requires high-pressure conditions but also suffers from byproducts such as sodium formate and sodium carbonate, which crystallize in the pipeline and cause blockages.[7] In addition, this technique is energy-consuming and environmentally unfriendly.[8] Recently, an electrocatalytic refinery strategy under ambient conditions as an eco- and energy-friendly alternative has gained much attention. Qiao et al. synthesized 2-chloroethanol through ethylene electro-oxidation with natural seawater as the electrolyte.[9,10] Accordingly, our proposed electrocatalytic oxidation coupling (EOC) strategy for the reaction of methanol and NH_3 provides a new and sustainable approach toward formamide synthesis (Figure 1a). However, both the activity and durability of catalytic materials under harsh oxidative conditions are still critical issues for EOC strategies, and the high dependence on noble metals to avoid dissolution of the catalyst further hinders their practical application.[11−13] Thus, it is highly desirable to develop functional transition metal (TM) materials with outstanding activity and stability for the EOC strategy, but this is still challenging.

Among the general methods for promoting the activity and stability of electrooxidation catalysts, including forming a protection layer, constructing superaerophobic nanoarrays, and doping heteroatoms, the doping strategy is the most facile and feasible due to its convenience and adjustability.[14−16] It has been reported that the unique electronic structure of rare earth elements enables highly active outermost f electrons and second-outermost d electrons, making them outstanding dopants.[17,18] Recently, rare earth element-doped materials have greatly increased the catalytic activity, energy conversion, and storage efficiency in multitudinous fields.[19−22] MnO_2 is particularly suitable as a catalytic material for electrooxidation due to its low price, eco-friendliness, and abundant resources.[23−25] Moreover, the electron configuration of manganese in MnO_2 is $3d^5 4s^2$, showing five electrons in unsaturated d orbitals, which is easy to electronically modulate and thus improves the catalytic activity and stability.[26,27] Therefore, rare earth element-doped MnO_2 is supposed to be a promising candidate for the EOC process to produce formamide but has rarely been reported.

Herein, various rare earth element-doped MnO_2 catalysts were synthesized by the pyrolysis method and used as electrooxidation catalysts for the C−N coupling of methanol and ammonia through the EOC process to synthesize

Received: September 12, 2023
Revised: October 6, 2023
Accepted: October 6, 2023
Published: October 19, 2023

https://doi.org/10.1021/jacsau.3c00537
JACS Au 2023, 3, 2987−2992

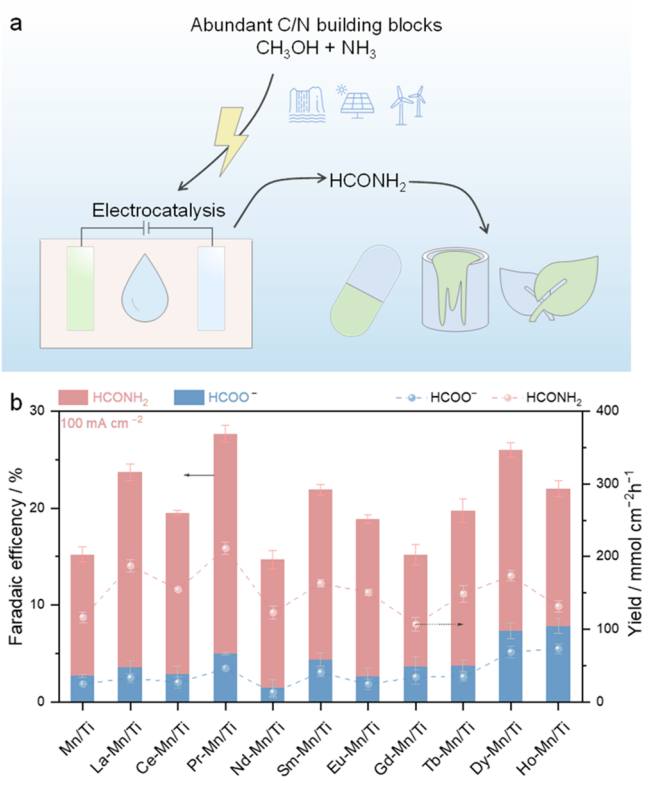

Figure 1. (a) Sustainable method to synthesize formamide from methanol and ammonia. (b) Catalyst screening.

formamide, among which Pr-doped MnO_2 (1%Pr-MnO_2) showed the best performance and stability enhancement. The optimized formamide production Faradaic efficiency (FE) and yield were 22.63% and 211.32 μmol cm^{-2} h^{-1}, respectively, which were able to maintain stability for more than 8 h. The key intermediates in the reaction process were captured by electrochemical online differential mass spectrometry (DEMS) and in situ attenuated total reflection Fourier transform infrared spectroscopy (ATR-FTIR). A reasonable reaction path was deduced. Our work not only demonstrates an efficient and stable non-noble catalyst for formamide electrosynthesis but also provides new insight into the application of rare earth metals as dopants to enhance the activity and stability of TM materials in electrooxidation reactions.

First, the performance of different catalysts for the EOC process to obtain formamide from methanol and ammonia was evaluated by electrolysis in a single-chamber electrolytic cell at a current density of 100 mA cm^{-2} for 3 h. Among the 11 screened materials, Pr-MnO_2 exhibited the highest FE of formamide, ~23%, which is approximately 2 times higher than that of the single MnO_2 counterpart, demonstrating that rare earth element doping could promote the EOC process toward formamide synthesis and that Pr is the best dopant from the perspective of formamide synthesis (Figure 1b). Thus, Pr-MnO_2 was chosen as the template material for further research.

To understand the physicochemical information on the chosen template material, a series of characterizations were performed by field-emission scanning electron microscopy (SEM), field-emission transmission electron microscopy (TEM), high-resolution TEM (HRTEM), X-ray diffraction (XRD), and X-ray photoelectron spectroscopy (XPS). As shown in Figures 2a and S1, the sintered Pr-MnO_2 and MnO_2 catalysts did not retain the lamellar structure but presented a

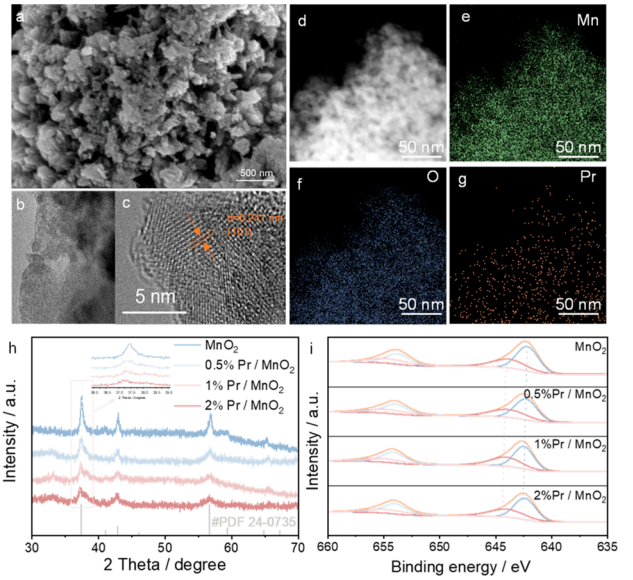

Figure 2. (a) SEM, (b) TEM, (c) HRTEM, and (d–g) EDS mapping of the Pr-MnO_2 catalyst. (h) XRD patterns of x%Pr-MnO_2. (i) XPS spectra of Pr-MnO_2 with different Pr loadings.

stacked three-dimensional configuration on top of each other. The higher-magnification TEM (Figures 2b and S2) showed that the Pr-MnO_2 edge structure is well-defined and that the internal structure is built up by lamellar layers. The lattice stripes of Pr-MnO_2 were characterized by HRTEM (Figure 2c), indicating that the exposed 101 crystal planes of Pr-MnO_2 possess larger crystal plane spacing compared to MnO_2(101) (Figure S2c), also suggesting that Pr is doped into the lattice rather than loaded on the surface of MnO_2. In addition, the uniform elemental distributions of Pr-MnO_2 and MnO_2 are confirmed by energy-dispersive spectroscopy (EDS) mapping (Figures 2d–g and S3).

To further illustrate the present form of Pr in the catalyst, we synthesized x%Pr-MnO_2 catalysts with different rare earth element contents (including x = 0, 0.5, 1, and 2) and characterized them by XRD and XPS. As shown in Figure 2h, the characteristic peaks in these four samples all originate from β-MnO_2 (JCPDS no. 24-0735), indicating that the introduced Pr does not affect the formation of the MnO_2-based material. Note that although the overall peaks remain unchanged, the main peak located at 37.5° shifts to a small angle with the introduction of Pr, and the shift becomes more obvious with the increased ratio of introduced Pr, further confirming that Pr with a larger atomic radius is doped into the MnO_2 crystal lattice.[28] Moreover, the XPS results (Figure 2i) show that the doping of Pr into MnO_2 results in a positive shift of binding energy in Mn^{4+} species with the doping amount of Pr, which reflects a deficiency of electrons on the Mn atoms in the doped MnO_2 materials, suggesting the existence of electronic interactions between Pr and MnO_2.[29,30] Although the XPS signal of Pr is relatively weak, the negative shift in binding energy further verifies the existence of electronic interactions and the high dispersion of the Pr dopant (Figure S4). All of these aforementioned results demonstrate that Pr is successfully doped into MnO_2.

Before evaluating the durability of the as-prepared Pr-MnO_2, we first optimized the reaction system by screening the volume ratio of methanol and ammonia at a current density of 100 mA cm^{-2} and found that the optimum performance was attained

https://doi.org/10.1021/jacsau.3c00537
JACS Au 2023, 3, 2987–2992

when the volume ratio was 2:1 (Figures 3a, S5, and S6). In addition, the performance of the catalysts with different rare

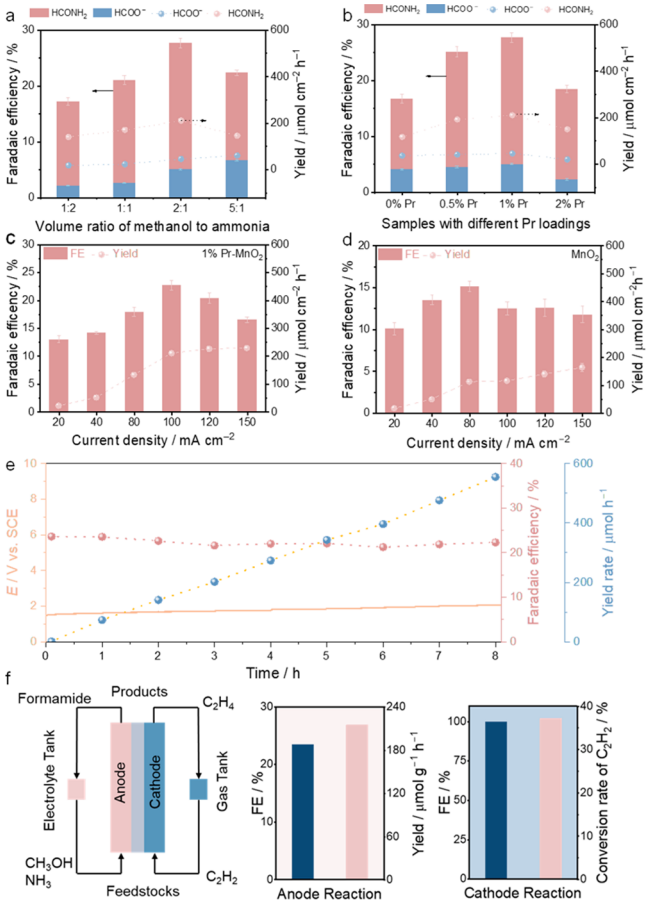

Figure 3. (a) Optimization of the volume ratio of methanol and ammonia. (b) Influence of different catalysts on formamide electrosynthesis. (c) Performance of 1% Pr-MnO_2. (d) Performance of MnO_2 for formamide synthesis. (e) Stability test of 1% Pr-MnO_2. (f) Illustration and performance of two-electrode electrolysis.

earth dopings was also compared with that of their MnO_2 counterparts, and it was discovered that the 1%Pr-MnO_2 catalyst demonstrates the highest selectivity toward formamide synthesis (Figure 3b). Then we conducted performance tests using 1%Pr-MnO_2 as the electrocatalyst at different current densities and compared the results with those for the control sample MnO_2. The optimal current densities for formamide production of 1%Pr-MnO_2 and MnO_2 were 100 and 80 mA cm^{-2}, with FEs of 22.63% and 15.13%, respectively (Figure 3c,d). The FE of all oxidation products under the optimized conditions is displayed in Figure S7. In addition, no-electricity control experiments were carried out to exclude the electrothermal effect (Figure S8). The stability evaluation of formamide electrosynthesis through the EOC process was performed under the optimal experimental conditions (CH_3OH:NH_3 = 2:1, 100 mA cm^{-2}). As shown in Figure S9, the FE and formamide yield of MnO_2 decrease immediately with the reaction time within 7.5 h, indicating the poor durability of the MnO_2 catalyst. Note that the formamide synthesis activity and selectivity of Pr-MnO_2 are retained after seven cycles of an 8 h continuous test (more than 50 h in total) without an obvious decay (Figures 3e, S10, and S11), confirming the enhanced catalytic durability after Pr doping. Moreover, MnO_2 needed a higher potential for stability testing under the same conditions, a significant potential rise occurred with increasing test time, and the catalyst was deactivated after less than 5 h of electrolysis, also indicating the poor conductivity and stability of the catalyst. The FE of formamide over MnO_2 gradually decreased and was less than one-half of the performance of Pr-MnO_2, further illustrating the importance of Pr doping for enhancing the activity and stability of MnO_2 used for formamide electrosynthesis (Figure S9). Additionally, we performed ICP analyses on the electrolyte following stability tests and discovered that the amount of Mn dissolved in Pr-MnO_2 is less than that of MnO_2 (Figure S12), which further reinforces that the doping of Pr is favorable for enhancing the durability of MnO_2. Moreover, a two-electrode flow electrolysis, which couples EOC with cathodic acetylene (C_2H_2) semihydrogenation to ethylene (C_2H_4) reaction,[31] was built to demonstrate the advantage of the electrocatalytic strategy. As shown in Figure 3f, C_2H_4 could be produced with a selectivity of ∼100% and a C_2H_2 conversion of 37.21% under the optimized conditions of the EOC process, further enhancing the additional value of our proposed electrocatalytic strategy.

To illustrate the changes in the catalyst during the reaction, we characterized the catalyst by using in situ Raman spectroscopy. As shown in Figure 4a, three distinct peaks

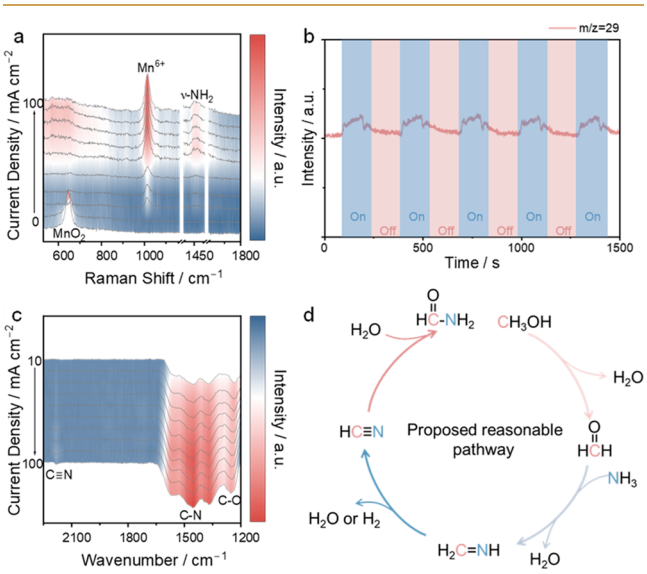

Figure 4. (a) In situ Raman, (b) DEMS, and (c) in situ ATR-FTIR spectra of 1% Pr-MnO_2. (d) Plausible reaction pathway.

located at 273, 367, and 646 cm^{-1} were attributed to MnO_2,[32,33] and with the application of current, the characteristic peak of MnO_2 disappeared and was subsequently replaced by a peak at 1014 cm^{-1} for Mn^{6+} species, which were regarded as the reactive sites.[34] Given the appearance of the surface-adsorbed *NH_2 peak signal (∼1450 cm^{-1}) at a relatively higher current density than that of the Mn^{6+} species, we rationally deduced that Mn^{6+} acted as a trigger for formamide electrosynthesis. To verify this assumption, an electricity cutoff control experiment was conducted. As shown in Figure S13, the intensity of the Mn^{6+} peak decreases quickly when the electricity is cut off, and the signal of *NH_2 disappears along with the Mn^{6+} species, confirming that the high-valence Mn^{6+} species play a key role in the oxidative coupling process, which

https://doi.org/10.1021/jacsau.3c00537
JACS Au 2023, 3, 2987−2992

is similar to Ni^{3+} in the oxygen evolution reaction.[35,36] Then, in situ Raman tests were also performed on MnO_2, and Mn^{6+} appeared only at a higher current density compared to Pr-MnO_2, indicating that the doping of Pr could favor the generation of Mn^{6+} during electrocatalysis. To further confirm the accuracy of the peak attribution, ex situ Raman tests of MnO_2, Pr-MnO_2, and carbon paper were carried out (see Figure S14 for details). Next, to reveal the reaction pathway of methanol and ammonia C−N coupling to formamide, we adopted online DEMS to trap the intermediate species of the reaction and found that the signal of the imine ($H_2C{=}NH_2$) intermediate with m/z = 29 was successfully captured with the application of current, which played a key role in the presumption of the reaction pathway (Figures 4b and S15).[37,38] To further investigate the changes in the intermediates during the reaction, we also performed in situ ATR-FTIR with the current density applied in the range of 10−100 mA cm^{-2}, during which the spectral signals were collected and the C−O (1245 cm^{-1}), C−N (1445 cm^{-1}), and C≡N (2183 cm^{-1}) signals of key intermediate species were successfully traced (Figure 4c).[39−41] Then a series of control experiments demonstrated that the HCOH intermediate and NH_3 reactant are crucial to the oxidative C−N strategy (Table S1). Thus, we propose a reasonable reaction pathway in which ammonia nucleophilically attacks the aldehyde intermediate produced by methanol oxidation, followed by dehydration to produce $H_2C{=}NH_2$, which is subsequently oxidized to produce HC≡N, hydrolysis of which yields formamide (Figure 4d).[42−44]

In conclusion, to overcome the noble metal dependence of the proposed ECO process, rare earth element-doped MnO_2-based materials were demonstrated as efficient, selective, and durable non-noble catalysts for the EOC process to form formamide with commendable activity and stability. The study demonstrates that the 1% Pr-doped MnO_2 catalyst can generate formamide at a current density of 100 mA cm^{-2} with a Faradaic efficiency of 22.63%, a yield of 211.32 mol cm^{-2} h^{-1}, and stability for 8 h. The easier formation of Mn^{6+} species and the lower dissolution rate of Mn species after Pr doping are revealed to be responsible for the boosted formamide production and enhanced stability. Additionally, we proposed a plausible C−N coupling reaction path and detected the key intermediates in the reaction process using methods such as DEMS and ATR-FTIR. This study not only offers a integrated method for the environmentally friendly synthesis of formamide and ethylene but also provides a fresh perspective into the application of rare earth metals as dopants to enhance the activity and stability of TM materials in electrooxidation reactions.

METHODS

Electrochemical Measurements

To begin the performance evaluation, pre-experiments on the electrolyte choice were conducted first. The target product was strongly suppressed in both strongly alkaline and acidic electrolytes. Thus, CH_3OH and NH_3 with different volume ratios were added to a 0.5 M $NaHCO_3$ aqueous solution. [Re]-MnO_2, Pt foil, and a saturated calomel electrode were used as the working, counter, and reference electrodes, respectively. Different current densities from 20 to 150 mA cm^{-2} were determined using an electrochemical workstation (CS150H, Wuhan CorrTest Instruments Co., Ltd.), and the reaction time was set as 3 h. The influence of the reactant ratio on the catalytic performance was determined by controlling the total volume of 15 mL (a mixture of CH_3OH and NH_3), and other experimental conditions were kept consistent. The two-electrode flow electrolyte electrochemical measurements were carried out in a typical membrane electrode reactor consisting of 1% Pr-MnO_2 as the working electrode and a gas diffusion layer (GDL) loaded with Cu nanoparticles as the counter electrode. The cathode cell and anode cell were separated by a Nafion 117 proton exchange membrane. A schematic illustration of the flow cell is shown in Figure 3f. A peristaltic pump was applied to implement circulation of the liquid phase. The flow rate of C_2H_2 gas was controlled at 15 mL min^{-1} by a mass flow meter, and the gas at the flow cell outlet was directly introduced into the gas chromatograph for the analysis of the products.

In Situ ATR-FTIR Measurements

In situ ATR-FTIR was carried out to trace the signals of the intermediates using a Nicolet Nexus 670 spectrometer equipped with a liquid-nitrogen-cooled mercury−cadmium−telluride detector. An ECIR-II cell equipped with a Pike Veemax III ATR accessory in a three-electrode system was provided by Shanghai Linglu Instrument & Equipment Co. The data were collected through Pt-covered monocrystal silicon. To improve the signal intensity, monocrystalline silicon was initially coated with a layer of Au using the chemical plating method.

ASSOCIATED CONTENT

Supporting Information

The Supporting Information is available free of charge at https://pubs.acs.org/doi/10.1021/jacsau.3c00537.

Additional experimental details, material characterizations, and methods, including the calibration curves (PDF)

AUTHOR INFORMATION

Corresponding Authors

Bin Zhang − *Department of Catalysis Science and Engineering, School of Chemical Engineering and Technology, Tianjin University, Tianjin 300072, China; Institute of Molecular Plus, Department of Chemistry, School of Science, Tianjin University, Tianjin 300072, China;* orcid.org/0000-0003-0542-1819; Email: bzhang@tju.edu.cn

Bo-Hang Zhao − *Institute of Molecular Plus, Department of Chemistry, School of Science, Tianjin University, Tianjin 300072, China*; Email: bhzhao@tju.edu.cn

Authors

Jiewei Zhu − *Department of Catalysis Science and Engineering, School of Chemical Engineering and Technology, Tianjin University, Tianjin 300072, China*

Jiang Shao − *Institute of Molecular Plus, Department of Chemistry, School of Science, Tianjin University, Tianjin 300072, China*

Bai-An Shen − *Institute of Molecular Plus, Department of Chemistry, School of Science, Tianjin University, Tianjin 300072, China*

Jixiang Chen − *Department of Catalysis Science and Engineering, School of Chemical Engineering and Technology, Tianjin University, Tianjin 300072, China;* orcid.org/0000-0003-2940-137X

Yifu Yu − *Institute of Molecular Plus, Department of Chemistry, School of Science, Tianjin University, Tianjin 300072, China;* orcid.org/0000-0002-7927-1350

Shuyan Song − *State Key Laboratory of Rare Earth Resources Utilization, Changchun Institute of Applied Chemistry,*

https://doi.org/10.1021/jacsau.3c00537
JACS Au 2023, 3, 2987−2992

Chinese Academy of Sciences, Changchun 130022, China; orcid.org/0000-0002-7758-752X

Xin-Bo Zhang − *State Key Laboratory of Rare Earth Resources Utilization, Changchun Institute of Applied Chemistry, Chinese Academy of Sciences, Changchun 130022, China;* orcid.org/0000-0002-5806-159X

Complete contact information is available at: https://pubs.acs.org/10.1021/jacsau.3c00537

Author Contributions

CRediT: **Jiewei Zhu** data curation, formal analysis, investigation, methodology; **Jiang Shao** formal analysis, methodology, validation, writing-original draft; **Bai-An Shen** formal analysis, investigation; **Jixiang Chen** formal analysis; **Yifu Yu** funding acquisition, resources, visualization, writing-review & editing; **Shuyan Song** data curation, investigation, project administration; **Xin-Bo Zhang** data curation, investigation, project administration; **Bin Zhang** conceptualization, formal analysis, supervision, writing-review & editing; **Bo-Hang Zhao** data curation, formal analysis, investigation, methodology, project administration, supervision, writing-original draft.

Notes

The authors declare no competing financial interest.

■ ACKNOWLEDGMENTS

We acknowledge the National Natural Science Foundation of China (22271213 and 22209120) and the Open Funds of the State Key Laboratory of Rare Earth Resource Utilization (RERU2022005).

■ REFERENCES

(1) Pattabiraman, V. R.; Bode, J. W. Rethinking Amide Bond Synthesis. *Nature* **2011**, *480*, 471−479.
(2) Tao, Z.; Rooney, C. L.; Liang, Y.; Wang, H. Accessing Organonitrogen Compounds via C-N Coupling in Electrocatalytic CO_2 Reduction. *J. Am. Chem. Soc.* **2021**, *143*, 19630−19642.
(3) Li, J.; Zhang, Y.; Kuruvinashetti, K.; Kornienko, N. Construction of C-N Bonds from Small-Molecule Precursors through Heterogeneous Electrocatalysis. *Nat. Rev. Chem.* **2022**, *6*, 303−319.
(4) Xu, J.; Chen, X.; Xu, Y.; Du, Y.; Yan, C. Ultrathin 2D Rare-Earth Nanomaterials: Compositions, Syntheses, and Applications. *Adv. Mater.* **2020**, *32*, 1806461.
(5) Meng, N.; Shao, J.; Li, H.; Wang, Y.; Fu, X.; Liu, C.; Yu, Y.; Zhang, B. Electrosynthesis of Formamide from Methanol and Ammonia under Ambient Conditions. *Nat. Commun.* **2022**, *13*, 5452.
(6) Guo, C.; Zhou, W.; Lan, X.; Wang, Y.; Li, T.; Han, S.; Yu, Y.; Zhang, B. Electrochemical Upgrading of Formic Acid to Formamide via Coupling Nitrite Co-Reduction. *J. Am. Chem. Soc.* **2022**, *144*, 16006−16011.
(7) Lv, C.; Lee, C.; Zhong, L.; Liu, H.; Liu, J.; Yang, L.; Yan, C.; Yu, W.; Hng, H. H.; Qi, Z.; Song, L.; Li, S.; Loh, K. P.; Yan, Q.; Yu, G. A Defect Engineered Electrocatalyst that Promotes High-Efficiency Urea Synthesis under Ambient Conditions. *ACS Nano* **2022**, *16*, 8213−8222.
(8) Tang, C.; Zheng, Y.; Jaroniec, M.; Qiao, S. Z. Electrocatalytic Refinery for Sustainable Production of Fuels and Chemicals. *Angew. Chem., Int. Ed.* **2021**, *60*, 19572−19590.
(9) Gao, Y.; Ge, L.; Xu, H.; Davey, K.; Zheng, Y.; Qiao, S. Z. ElectroCatalytic Refinery of Biomass-Based 5-Hydroxymethylfurfural to Fine Chemicals. *ACS Catal.* **2023**, *13*, 11204−11231.
(10) Huang, L.; Wang, P.; Jiang, Y.; Davey, K.; Zheng, Y.; Qiao, S. Z. Ethylene Electrooxidation to 2-Chloroethanol in Acidic Seawater with Natural Chloride Participation. *J. Am. Chem. Soc.* **2023**, *145*, 15565−15571.
(11) Jiao, Y.; Li, H.; Jiao, Y.; Qiao, S. Activity and Selectivity Roadmap for C-N Electro-Coupling on MXenes. *J. Am. Chem. Soc.* **2023**, *145*, 15572−15580.
(12) Chen, F.-Y.; Wu, Z.-Y.; Adler, Z.; Wang, H. Stability Challenges of Electrocatalytic Oxygen Evolution Reaction: From Mechanistic Understanding to Reactor Design. *Joule* **2021**, *5*, 1704−1731.
(13) Song, J.; Wei, C.; Huang, Z.-F.; Liu, C.; Zeng, L.; Wang, X.; Xu, Z. J. A Review on Fundamentals for Designing Oxygen Evolution Electrocatalysts. *Chem. Soc. Rev.* **2020**, *49*, 2196−2214.
(14) Rochlitz, L.; Fischer, J. W. A.; Pessemesse, Q.; Clark, A. H.; Ashuiev, A.; Klose, D.; Payard, P.-A.; Jeschke, G.; Copéret, C. Ti-Doping in Silica-Supported PtZn Propane Dehydrogenation Catalysts: From Improved Stability to the Nature of the Pt−Ti Interaction. *JACS Au* **2023**, *3*, 1939−1951.
(15) Wang, P. C.; Jia, T.; Wang, B. G. A Critical Review: 1D/2D Nanostructured Self-Supported Electrodes for Electrochemical Water Splitting. *J. Power Sources* **2020**, *474*, 228621.
(16) Kim, Y.; Jung, S.-M.; Kim, K.-S.; Kim, H.-Y.; Kwon, J.; Lee, J.; Cho, H.-S.; Kim, Y.-T. Cathodic Protection System against a Reverse-Current after Shut-Down in Zero-Gap Alkaline Water Electrolysis. *JACS Au* **2022**, *2*, 2491−2500.
(17) Wu, Y.; Zhao, J.; Wang, C.; Li, T.; Zhao, B. H.; Song, Z.; Liu, C.; Zhang, B. Electrosynthesis of a Nylon-6 Precursor from Cyclohexanone and Nitrite under Ambient Conditions. *Nat. Commun.* **2023**, *14*, 3057.
(18) Zheng, B.; Fan, J.; Chen, B.; Qin, X.; Wang, J.; Wang, F.; Deng, R.; Liu, X. Rare-Earth Doping in Nanostructured Inorganic Materials. *Chem. Rev.* **2022**, *122*, 5519−5603.
(19) Kim, C.; Dionigi, F.; Beermann, V.; Wang, X.; Möller, T.; Strasser, P. Alloy Nanocatalysts for the Electrochemical Oxygen Reduction (ORR) and the Direct Electrochemical Carbon Dioxide Reduction Reaction (CO_2RR). *Adv. Mater.* **2019**, *31*, 1805617.
(20) Escudero-Escribano, M.; Malacrida, P.; Hansen, M. H.; Vej-Hansen, U. G.; Velázquez-Palenzuela, A.; Tripkovic, V.; Schiøtz, J.; Rossmeisl, J.; Stephens, I. E.; Chorkendorff, I. Tuning the Activity of Pt Alloy Electrocatalysts by Means of the Lanthanide Contraction. *Science* **2016**, *352*, 73−76.
(21) Liang, J.; Liu, P.; Li, Q.; Li, T.; Yue, L.; Luo, Y.; Liu, Q.; Li, N.; Tang, B.; Alshehri, A. A.; Shakir, I.; Agboola, P. O.; Sun, C.; Sun, X. Amorphous Boron Carbide on Titanium Dioxide Nanobelt Arrays for High-Efficiency Electrocatalytic NO Reduction to NH_3. *Angew. Chem., Int. Ed.* **2022**, *61*, No. e202202087.
(22) Liu, Z.; Li, N.; Zhao, H.; Zhang, Y.; Huang, Y.; Yin, Z.; Du, Y. Regulating the Active Species of $Ni(OH)_2$ using CeO_2: 3D CeO_2/$Ni(OH)_2$/Carbon Foam as an Efficient Electrode for the Oxygen Evolution Reaction. *Chem. Sci.* **2017**, *8*, 3211−3217.
(23) Chen, C.; Zhao, S.; Tang, X.; Yi, H.; Gao, F.; Yu, Q.; Liu, J.; Wang, W.; Tang, T.; Meng, X. δ-MnO_2 Decorated Layered Double Oxides In-Situ Grown on Nickel Foam towards Electrothermal Catalysis of n-Heptane. *J. Environ. Sci. (China)* **2023**, *126*, 308−320.
(24) Zhong, Y.; Xiong, H.; Low, J.; Long, R.; Xiong, Y. Recent Progress in Electrochemical C−N Coupling Reactions. *eScience* **2023**, *3*, 100086.
(25) Mang, C.; Li, G.; Rao, M.; Zhang, X.; Luo, J.; Jiang, T. An Ab Initio Investigation on the Mechanism of Formaldehyde Oxidation: A Case of Heterogeneous Catalytic Reaction over Graphene-Like MnO_2 Monolayer Anchored Different Single Atoms (Fe, Co, and Ni). *Appl. Surf. Sci.* **2023**, *608*, 154964.
(26) Zhang, C.; Li, M.; Wang, X.; Fan, L.; Dong, Y.; Zhu, Y. Excellent Oxidation Activity of Toluene over Core-Shell Structure Mn_2O_3@MnO_2: Role of Surface Lattice Oxygen and Mn Species. *J. Chem. Technol. Biotechnol.* **2022**, *97*, 1138−1148.
(27) Jouny, M.; Lv, J.-J.; Cheng, T.; Ko, B. H.; Zhu, J.-J.; Goddard, W. A.; Jiao, F. Formation of Carbon−Nitrogen Bonds in Carbon Monoxide Electrolysis. *Nat. Chem.* **2019**, *11*, 846−851.
(28) Ye, Z.; Li, T.; Ma, G.; Dong, Y.; Zhou, X. Metal-Ion (Fe, V, Co, and Ni)-Doped MnO_2 Ultrathin Nanosheets Supported on Carbon Fiber Paper for the Oxygen Evolution Reaction. *Adv. Funct. Mater.* **2017**, *27*, 1704083.

(29) Liu, T.; Yao, Y.; Wei, L.; Shi, Z.; Han, L.; Yuan, H.; Li, B.; Dong, L.; Wang, F.; Sun, C. Preparation and Evaluation of Copper-Manganese Oxide as a High-Efficiency Catalyst for CO Oxidation and NO Reduction by CO. *J. Phys. Chem. C* **2017**, *121*, 12757−12770.
(30) Yang, R.; Peng, S.; Lan, B.; Sun, M.; Zhou, Z.; Sun, C.; Gao, Z.; Xing, G.; Yu, L. Oxygen Defect Engineering of β-MnO_2 Catalysts via Phase Transformation for Selective Catalytic Reduction of NO. *Small* **2021**, *17*, No. 2102408.
(31) Zhao, B. H.; Chen, F.; Wang, M.; Cheng, C.; Wu, Y.; Liu, C.; Yu, Y.; Zhang, B. Economically Viable Electrocatalytic Ethylene Production with High Yield and Selectivity. *Nat. Sustain.* **2023**, *6*, 827−837.
(32) Abou-Rjeily, J.; Bezza, I.; Laziz, N. A.; Autret-Lambert, C.; Sougrati, M. T.; Ghamouss, F. High-Rate Cyclability and Stability of $LiMn_2O_4$ Cathode Materials for Lithium-Ion Batteries from Low-Cost Natural β-MnO_2. *Energy Storage Mater.* **2020**, *26*, 423−432.
(33) Ma, S.; Ye, X.; Jiang, X.; Cen, W.; Jiang, W.; Wang, H. First Principles Calculation of Mechanical, Dynamical and Thermodynamic Properties of MnO_2 with Four Crystal Phases. *J. Alloys Compd.* **2021**, *852*, 157007.
(34) Cao, R.; Qiu, J.; Yu, X.; Sun, X. Spectroscopic Investigation on $BaSO_4$:(Mn^{6+}, Mn^{5+}) Crystal. *ECS J. Solid State Sci. Technol.* **2013**, *2*, R237.
(35) Trotochaud, L.; Young, S. L.; Ranney, J. K.; Boettcher, S. W. Nickel-Iron Oxyhydroxide Oxygen-Evolution Electrocatalysts: the Role of Intentional and Incidental Iron Incorporation. *J. Am. Chem. Soc.* **2014**, *136*, 6744−6753.
(36) Huang, C.; Huang, Y.; Liu, C.; Yu, Y.; Zhang, B. Integrating Hydrogen Production with Aqueous Selective Semi-Dehydrogenation of Tetrahydroisoquinolines over a Ni_2P Bifunctional Electrode. *Angew. Chem., Int. Ed.* **2019**, *131*, 12142−12145.
(37) Sun, W.-J.; Ji, H.-Q.; Li, L.-X.; Zhang, H.-Y.; Wang, Z.-K.; He, J.-H.; Lu, J.-M. Built-In Electric Field Triggered Interfacial Accumulation Effect for Efficient Nitrate Removal at Ultra-Low Concentration and Electroreduction to Ammonia. *Angew. Chem., Int. Ed.* **2021**, *60*, 22933−22939.
(38) Shao, J.; Meng, N.; Wang, Y.; Zhang, B.; Yang, K.; Liu, C.; Yu, Y.; Zhang, B. Scalable Electrosynthesis of Formamide through C−N Coupling at the Industrially Relevant Current Density of 120 mA cm^{-2}. *Angew. Chem., Int. Ed.* **2022**, *61*, No. e202213009.
(39) Meng, N.; Zhou, W.; Yu, Y.; Liu, Y.; Zhang, B. Superficial Hydroxyl and Amino Groups Synergistically Active Polymeric Carbon Nitride for CO_2 Electroreduction. *ACS Catal.* **2019**, *9*, 10983−10989.
(40) Huang, Y.; Wang, Y.; Wu, Y.; Yu, Y.; Zhang, B. Electrocatalytic Construction of the C-N Bond from the Derivates of CO_2 and N_2. *Sci. China: Chem.* **2022**, *65*, 204−206.
(41) Chen, C.; He, N.; Wang, S. Electrocatalytic C−N Coupling for Urea Synthesis. *Small Sci.* **2021**, *1*, 2100070.
(42) Gunanathan, C.; Ben-David, Y.; Milstein, D. Direct Synthesis of Amides from Alcohols and Amines with Liberation of H_2. *Science* **2007**, *317*, 790−792.
(43) Oishi, T.; Yamaguchi, K.; Mizuno, N. Catalytic Oxidative Synthesis of Nitriles Directly from Primary Alcohols and Ammonia. *Angew. Chem., Int. Ed.* **2009**, *48*, 6286−6288.
(44) Yamaguchi, K.; Kobayashi, H.; Oishi, T.; Mizuno, N. Heterogeneously Catalyzed Synthesis of Primary Amides Directly from Primary Alcohols and Aqueous Ammonia. *Angew. Chem., Int. Ed.* **2012**, *51*, 544−547.

https://doi.org/10.1021/jacsau.3c00537
JACS Au 2023, 3, 2987−2992